

Diffuse Atomic and Molecular Gas near IC 443

A. Hirschauer¹, S. R. Federman², George Wallerstein³, and T. Means³

ABSTRACT

We present an analysis of results on absorption from Ca II, Ca I, K I, and the molecules CH⁺, CH, C₂, and CN that probes gas interacting with the supernova remnant IC 443. The eleven directions sample material across the visible nebula and beyond its eastern edge. Most of the neutral material, including the diatomic molecules, is associated with the ambient cloud detected via H I and CO emission. Analysis of excitation and chemistry yields gas densities that are typical of diffuse molecular gas. The low density gas probed by Ca II extends over a large range in velocities, from -120 to $+80$ km s⁻¹ in the most extreme cases. This gas is distributed among several velocity components, unlike the situation for the shocked molecular clumps, whose emission occurs over much the same range but as very broad features. The extent of the high-velocity absorption suggests a shock velocity of 100 km s⁻¹ for the expanding nebula.

Subject headings: ISM: abundances — ISM: kinematics and dynamics — ISM: molecules — ISM: supernova remnants (IC 443)

1. Introduction

IC 443 seems to be an example of the interaction of a supernova remnant (SNR) with an interstellar cloud or complex of clouds. As such it provides the opportunity to observe the effects of the SN shock penetrating the high density gas of the clouds. This involves heating the cloud to x-ray temperatures, followed by rapid cooling leading to a significant increase in the cloud's density. IC 443 has been a very popular target and comparison object primarily for x-ray observations and as an object with emission by excited molecules. According to

¹Department of Physics, University of Notre Dame, Notre Dame, IN 46556.

²Department of Physics and Astronomy, University of Toledo, Toledo, OH 43606; steven.federman@utoledo.edu

³Department of Astronomy, University of Washington, Seattle, WA 98195; wall@astro.washington.edu

SIMBAD there have been 619 published studies or references to published studies between 1850 and 2007.

IC 443 has provided an opportunity to compare observations and theory of the hydrodynamics and radiative transfer associated with the penetration of clouds by a SN shock. Specific calculations were first made by McKee & Cowie (1975) and reviewed by Chevalier (1977). Early detailed spectroscopic observations of absorption from the SN shocked clouds associated with the Vela Remnant were described by Jenkins, Silk, & Wallerstein (1976). Here we describe measurements on atomic and molecular absorption seen in the spectra of stars behind IC 443 and attempt to link them to the wealth of results already available.

Observations of SNRs may be made by a wide variety of instruments each of which defines the spectral resolution, spectral coverage, and spatial resolution. We present new data on interstellar (IS) absorption from atoms and molecules at visible wavelengths. Such observations provide the finest spatial resolution and high spectral resolution, but are limited by the availability of background stars. The stars must be of sufficient brightness and have a relatively simple absorption spectrum to permit a clear definition of the IS features. Members of the Gem OB1 association afford us the opportunity to probe significant portions of the sky in the vicinity of IC 443.

Early molecular observations with good spatial resolution of phenomena associated with IC 443 were obtained by Cornett, Chen, & Knapp (1977) and Scoville et al. (1977) using the CO line at 2.6 mm. The former achieved a resolution of $24'' \times 27''$ while the latter had a half-power beamwidth of $2'$. Both studies compared their contours with the red image of the Palomar Sky Survey where the emission is dominated by H-alpha. The strongest emission was observed to come from the region between the two most prominent H-alpha emitting clouds, hinting that the CO was associated with a molecular cloud rather than with the nearby H II regions. In fact most papers since then have referred to IC 443 as the interaction of a SNR with a molecular cloud. As such it is probably the most readily observable example of an SNR associated with a molecular cloud because both the Vela Remnant and the Cygnus Loop seem to involve atomic gas with only a small amount of associated molecules.

Two papers within the past few years have attracted attention to IC 443 once again. Snell et al. (2005) used the *Submillimeter Wave Astronomy Satellite* to observe previously inaccessible lines of H₂O, O₂, C I, and ¹³CO along with ground-based observations of CO and HCO⁺. The authors invoke a combination of a fast J-type shock with velocity of about 100 km s⁻¹ and a slow shock (10 to 20 km s⁻¹) that could be either J-type or C-type. Using the Very Large Array and Arecibo telescopes Lee et al. (2008) observed 21 cm H I emission with a resolution of 40 arcseconds, comparable to that of the CO emission of Cornett et

al. H I emission with a velocity range from -100 to $+50$ km s $^{-1}$ was found. The systemic velocity was -5 km s $^{-1}$, like that found for the ambient molecular cloud. The high spectral resolution allowed Lee et al. to resolve the shocked H I into filaments, and they proposed that the main shock propagated through a uniform medium before reaching the edge of the cloud and freely expanding toward the southeast. Much of the H I emission in the northeast portion was attributed to recombining gas behind the shock front, while the southern emission was coincident with the dissociative molecular shock.

Our main goal is to examine how results from atomic and molecular absorption fit into the above picture. We also build upon the earlier measurements on absorption from Na I D and Ca II K by Welsh & Sallmen (2003), who studied four stars at relatively high spectral resolution. They detected absorption from numerous components over a velocity range from -100 to $+50$ km s $^{-1}$, much like that seen in H I emission. Our sample enlarges the number of sight lines probed and incorporates measurements on Ca I, K I, and the molecular species CH $^+$, CH, C $_2$, and CN. These species help us make connections between the diffuse molecular gas and the ambient molecular cloud. The result is a more complete understanding of the interaction between a SN shock and a molecular cloud.

2. Observations

Observations were obtained with the echelle spectrograph of the 3.5-m telescope of the Apache Point Observatory on 21 March and 28 December of 2006, 5 and 28 January of 2007, and 3 January of 2008. Our targets are listed in Table 1, along with pertinent stellar data. The coordinates and spectral type, as well as the V and $B - V$ magnitudes, are from the SIMBAD database, operated by CDS, Strasbourg, France. The absolute magnitude and reddening are derived from these data (see Böhm-Vitense 1981). Figure 1 displays the position of the lines of sight relative to CO contours of Huang, Dickman, & Snell (1986). The extent of the radio continuum emission is indicated by the dashed line. Bias frames, flat fields, and Th-Ar comparison spectra were acquired each night. The bias subtracted, flat fielded, wavelength calibrated, one-dimensional spectra were extracted with IRAF routines. Doppler corrections were applied to bring the spectra into the frame of the Local Standard of Rest. All spectra have a resolving power of about 35,000 and a signal-to-noise ratio from about 200 at 8000 Å declining slowly to between 50 and 100 at the CN lines near 3875 Å. Representative spectra appear in Figures 2 to 4.

The moderate-resolution spectra offered a glimpse at the component structure for the directions probing the vicinity of IC 443. Using standard routines in the IRAF environment, we extracted equivalent widths (W_λ) in the following way. We started the process by obtain-

ing the structure seen in the K I $\lambda 7699$ spectra; the features are relatively strong and many of the components are present. We then found the amount of absorption from the species showing much weaker absorption (Ca I and the molecules CH, CH⁺, CN, and C₂), making certain of the reality of these components by requiring consistency in v_{LSR} among the species in light of the spectral resolution. The high-resolution study by Pan et al. (2004) helped us determine the expected correspondences. The last step involved the extraction of the Ca II components. The availability of lines from both Ca II H and K aided the process, especially when the number of components was much greater than seen in other species. The Ca II absorption toward HD 43582 was particularly challenging; in this case we were guided by the results from Welsh & Sallmen (2003), but we note that our final component structure differed somewhat from theirs. Our survey does not incorporate results on the Na I D lines; the substantial optical depth at line center and our coarse spectral resolution did not allow meaningful interpretation. Tables 2 and 3 present the compilation of our set of $W_{\lambda s}$.

Special care is required when deriving column densities from spectra that may contain unresolved component structure. We applied several methods to minimize the potential impact of unresolved structure. First, the ‘effective’ b -value for the dominant, molecule-bearing components was determined by requiring the absorption from K I $\lambda 7699$ and from the much weaker doublet at 4044 and 4047 Å, which was seen toward HD 254755, to yield the same column density. Because many of the lines are not optically thin, this was necessary to account for optical depth effects in curves of growth. A self-consistent column density indicated an ‘effective’ b -value of 2.2 km s⁻¹. The detailed analysis of component structure in Ca II, Ca I, K I, CH⁺, CH, and CN by Pan et al. (2005) revealed a typical b -value for K I lines of 1 km s⁻¹, suggesting that unresolved structure is indeed present in our spectra. It appears that there are two components separated by about 2 km s⁻¹ hidden within the features seen in our data. According to Pan et al. (2005), K I, Ca I, CH, and CN lines have comparable b -values, and we adopted a b -value of 2.2 km s⁻¹ for the latter three species in an analysis based on curves of growth. For CH⁺, whose typical b -value is somewhat larger (Pan et al. 2005), we chose $b = 2.5$ km s⁻¹. The suite of molecular oscillator strengths used here comes from (Federman et al. 1994) and the atomic f -values are from Morton (1991), for consistency with our earlier work. The differences with Morton (2003) are only at the level of a few percent.

Second, the complete spectra afforded by the echelle spectrograph allowed us to compare results from strong and weak lines from CH⁺, CH, C₂, and CN. In particular, there are (1) CH⁺ $\lambda\lambda 3957, 4232$, (2) the $A - X$ and $B - X$ transitions in CH, (3) P, Q, and R lines for C₂, and (4) the P and R lines of CN. Furthermore for CH, the lines at 3878 and 3890 Å arise from the same Λ -doubling component of the ground state, and earlier studies at visible wavelengths (Danks, Federman, & Lambert 1984; Lien 1984; Jura & Meyer 1985) indicate

that the populations for both Λ -doubling components are the same. Thus, the column density obtained from $\lambda 3886$ should equal that from the two lines of the other Λ -doubling component. Within the mutual uncertainties of the features detected in our spectra, self-consistent column densities are obtained in all cases. In the cases of C_2 and CN, where absorption from multiple rotational levels is seen, total column densities are also obtained for the chemical analyses described below. The summary of results for C_2 is given in Table 4. When only $J = 4$ shows detectable absorption, or when absorption is only seen for $J = 0$ to 4, the total C_2 column density is estimated from the distribution of levels seen toward HD 254577. In the former case, the result for $J = 4$ is multiplied by 3.3, while the sum for $J = 0$ to 4 is multiplied by 1.5 in the latter. When comparison is made with high-quality results based on the $D - X$ (0,0) band at 2313 Å (Lambert, Sheffer, & Federman 1995; Sonnentrucker et al. 2007), the multiplicative factors yield total column densities that are 25-40% smaller. However, most of the difference arises from levels with $J > 10$. When only the $J = 0$ line of CN is detected, the CN column density is inferred by multiplying the result for the ground state by 1.5, a result consistent with excitation from the 2.7 K Cosmic Background.

For Ca II H and K, we adopted the Doublet Ratio Method (Strömgren 1948; Münch 1968). A listing of the set of column densities for each component seen in Ca II absorption appears in Table 5; the velocities come from the results for Ca II K. A comparison of the Ca II column densities toward HD 254577, HD 43582, and HD 254755 found by Welsh & Sallmen (2003) generally shows reasonable agreement, with the most optically thick velocity components agreeing to better than 50%. With our limited spectral resolution and their limited signal-noise, better correspondence cannot be expected.

3. Results and Discussion

3.1. General Results

Before describing specifics, we note some general findings. The most widespread absorption is found on the eastern portion of the remnant. The Ca II spectra seen toward HD 254477, HD 254577, and HD 43582 reveal components spanning the range from -120 to $+80$ km s $^{-1}$ (in the case for HD 43582). Moreover, Ca II features are present at -75 km s $^{-1}$ toward HD 254346, HD 254755, and HD 43907; these directions are relatively close to the three sight lines with the widest ranges in velocity components (see Fig. 1). The remaining directions in our survey probe more northern material. While absorption from the neutrals, Ca I and K I, is more restricted, there are components at -80 km s $^{-1}$. On the other hand, most of the molecular absorption occurs at low velocities (between -10 and $+10$ km s $^{-1}$).

The main components at slightly negative velocities correspond to the ambient gas detected via H I (Lee et al. 2008) and CO emission (Cornett et al. 1977; Scoville et al. 1977) and to the peaks seen in CO emission from the preshock molecular clumps (e.g., Huang et al. 1986; Dickman et al. 1992). CH⁺ is also detected at intermediate velocities (–25 to –75 km s^{–1}) toward HD 254477, HD 254577, and HD 43703, which comes as a surprise.

General trends are also seen in abundances. Some of the Ca I lines are relatively strong with $W_\lambda \sim 10$ mÅ and in the case of the –1.2 km s^{–1} component toward HD 254477, it is very strong ($W_\lambda \sim 50$ mÅ). The ratio of Ca I to Ca II column densities, however, is within a factor of a few of 0.01, which is typical of the general ISM (Welty, Hobbs, & Morton 2003). This atomic material probably has gas densities of about 10 cm^{–3}, as suggested by the analysis of H I emission (Lee et al. 2008). Significant amounts of molecular absorption are seen in many directions, indicating that diffuse molecular gas lies beyond the CO contours in the map of Huang et al. (1986) and even the contours of the ambient cloud (Cornett et al. 1977; Scoville et al. 1977). The most molecular rich diffuse gas, as revealed by CN, appears to be associated with clumps B, C, and D (Huang et al. 1986). HD 43582 must lie in front of clump H because C₂ and CN are not detected. Finally, we note that HD 43871 lies in front of IC 443; this sight line contains but small amounts of Ca II and K I, a result consistent with the much lower reddening toward the star.

3.2. Molecular Analysis

Our spectra allow us to derive the physical conditions, gas density and temperature and the flux of ultraviolet (UV) radiation permeating the cloud(s), from the distribution of C₂ rotational levels and from the chemistry involving CH, C₂, and CN. We adopted the method of Federman et al. (1994), with updates given in our more recent papers (e.g., Pan et al. 2005). The discussion in Sheffer et al. (2008) provides a sense of the limitations associated with the chemical analysis. Since we are seeking densities good to a factor of two, these limitations are less of a concern here.

3.2.1. C₂ Excitation

The excitation of C₂ molecules arises from a combination of collisions, which mainly affects the populations of low-lying rotational levels, and pumping via infrared photons to excited electronic states followed by cascades (van Dishoeck & Black 1982). Our focus is on determinations of gas density and temperature. We compared in a least-squares fashion

the observed rotational populations relative to the population in $J = 2$ with the predicted ratios from van Dishoeck (1984), whose tables of results are more extensive than those of van Dishoeck & Black (1982). The outcome is the parameter, $n \sigma_o / I_{ir}$, for a given kinetic temperature. Here, the density of collision partners, n , equals $n(\text{H}) + n(\text{H}_2)$, σ_o is the cross section for collisional de-excitation, and I_{ir} is the enhancement in the infrared flux relative to the average interstellar value. We continue to use a cross section of $2 \times 10^{-16} \text{ cm}^2$ (van Dishoeck & Black 1982), but note that the calculations of Lavendy et al. (1991), Robbe et al. (1992), and Najjar et al. (2008) indicate values a factor of two larger. We also assume that there is no enhancement in the infrared radiation field ($I_{ir} = 1$). Since we are interested in the gas density, $n_H = n(\text{H}) + 2 n(\text{H}_2)$, we multiply n by 1.5, as we have done in the past. Finally, we have to take into account the fact that we used slightly smaller oscillator strengths for the $A - X$ electronic transitions. [Our band oscillator strength of 1×10^{-3} is within $1\text{-}\sigma$ of the recommended revised value of Lambert et al. (1995).] Our densities are divided by 1.6 to account for this difference. The analysis provides values for gas densities that are known to a factor of two and for kinetic temperatures that are consistent with the relative populations in the lowest rotational levels.

We obtained results for several rotational levels toward ALS 8828, HD 254346, HD 254577, and HD 254755. However, the results for ALS 8828 were not especially meaningful. For the other three sight lines, we infer kinetic temperatures and gas densities of 30 to 60 K and 200 to 450 cm^{-3} , 10 to 60 K and 200 to 450 cm^{-3} , and 30 to 40 K and 200 cm^{-3} for the diffuse molecular gas toward HD 254346, HD 254577, and HD 254755, respectively. Such values are typically found for diffuse material, but the densities are significantly lower than the values derived for the preshock molecular gas, 3000 to 10^4 cm^{-3} , by Ziurys, Snell, & Dickman (1989) and van Dishoeck, Jansen, & Phillips (1993) from molecular emission. This is not unexpected considering the critical densities needed for molecular emission.

3.2.2. Chemistry

This analysis is based on a set of algebraic expressions describing the rate equations for C_2 and CN (e.g., Federman et al. 1994; Pan et al. 2005; Sheffer et al. 2008). Here the main outcome is gas density known again to a factor of 2. The reaction rate coefficients, rates for photoprocessing, and the fractional abundances for C^+ , N , and O are from our recent work. A kinetic temperature of 60 K is used, but the value does not greatly affect the outcome for gas density. The flux of UV radiation impinging on the cloud is taken to be the average interstellar value (i.e., $I_{uv} = 1$). This leaves the optical depth at 1000 \AA for grain attenuation, τ_{uv} , as the one significant unknown parameter for each line of sight. The UV extinction seen

toward HD 43818, another member of the Gem OB1 association, by Savage et al. (1985) and Valencic, Clayton, & Gordon (2004) indicates that a typical Galactic extinction law applies. Thus, we used $\tau_{uv} = 2 \times 3.1 \times E(B - V)$ in our calculations. The observed column densities of CH and CN, as well as C₂ when available, are input for the algebraic expressions, and a least-squares analysis that matched observed and predicted CN and C₂ column density yields gas density. Before doing so however, two additional issues had to be addressed.

Since the stars are about 1500 pc away, we also had to estimate the amount of extinction from foreground material not participating in the interaction with IC 443. We considered the following points. First, most of the CH and all of the C₂ and CN absorption arises from the ambient cloud at velocities near -5 km s^{-1} . This cloud also has at least 85% of the K I column along the lines of sight. Second, we obtained the amount of Na I D not at the velocity of the ambient molecular gas from the measurements of Welsh & Sallmen (2003) for HD 43582. This sight line, without detectable amounts of CN and $E(B - V)$ of about 0.60, contains about half the Na I in the molecular velocity component. We then suggest that a foreground contribution of $E(B - V) = 0.30$ ($\tau_{uv} = 1.86$) applies to the CN-rich directions in our sample.

Finally, we took into account that some of the CH was associated with CH⁺ synthesis in low density gas ($n_H < 100 \text{ cm}^{-3}$), not the chemistry of CN (e.g., Lambert, Sheffer, & Crane 1990; Pan et al. 2005). The components revealing only absorption from CH and CH⁺ were used to correct for this chemical route. For these components, the average $N(\text{CH}^+)/N(\text{CH})$ ratio was 0.43 ± 0.03 . For the molecular-rich components at -5 km s^{-1} , we reduced the CH column density by the CH associated with CH⁺ using the above ratio. The procedure lowered $N(\text{CH})$ by 20 to 50%.

In the course of performing this analysis, we were not able to find a reasonable solution ($n_H \leq 1600 \text{ cm}^{-3}$) by matching the values of $N(\text{C}_2)$ given in Table 5. It appeared that the values for $N(\text{C}_2)$ were all too high. Placing the present results on the plots of $N(\text{CN})$ versus $N(\text{CH})$, $N(\text{C}_2)$ versus $N(\text{CH})$, and $N(\text{CN})$ versus $N(\text{C}_2)$ given by Federman et al. (1994) revealed an interesting trend. Our C₂ results for the sight lines through IC 443 were not distributed uniformly about the best fit, while those of CN were. It appears that our derived C₂ column densities are too high by a factor of a few, but we cannot discern the cause. As a result, we restricted the analysis to reproducing the CN column densities. It is important to note, however, that the analysis of C₂ excitation above is not affected by this multiplicative factor because it relies on relative populations.

The restricted chemical analysis is able to reproduce the observed values for CN with gas densities of 200 to 400 cm^{-3} for most of the sight lines (ALS 8828, HD 254346, HD 254577, HD 254755, HD 43703, and HD 43907). This range in density agrees very well with the

results of C_2 excitation for the directions toward HD 254346, HD 254577, and HD 254755. The lone exception is the molecular gas toward HD 254477, where the inferred density is about a factor of 2 higher. This may arise because of our sight lines, only this direction passes within a contour for a clump (B – see Fig. 1). (Since there is no CN detected toward HD 43582, this star must lie in front of clump H). It seems that the material probed by our measurements represents the diffuse (molecular) envelope of the ambient cloud.

3.3. High-velocity Gas

We arbitrarily define “high-velocity gas” as deviating from the local velocity of -5 km s^{-1} for IC 443 by more than 25 km s^{-1} . Galactic rotation should not contribute high velocity components since the Galactic longitude of IC 443 is 189° . High-velocity gas is seen mostly in Ca II and predominantly with negative velocities, indicating expansion from the center of the system toward the Sun. Three stars show high velocity Ca I and two stars show it in the K I line, which is rather unusual. High velocity CH^+ is seen toward HD 254477 and HD 43703. No other molecular lines reveal high-velocity absorption. The only star to show high positive velocity gas is HD 43582. The $N(\text{Ca I})/N(\text{Ca II})$ ratio and the presence of the CH^+ molecule indicate that the high-velocity gas is associated with low densities.

Some comparison with 21 cm emission is possible, though the beam size, even with an interferometer, was 21×56 arcseconds in the survey of Braun & Strom (1986). In at least one case it is possible to compare 21 cm emission and optical absorption data. As shown in their Fig. 7, they detect emission with velocities up to -105 km s^{-1} at $\alpha(1950) = 6^h 14^m 16^s$, $\delta(1950) = 22^\circ 30' 14''$, which is fairly close to HD 254477 (see our Fig. 1 in 1950 coordinates). That star shows Ca II absorption components at -64.5 , -77.6 , -91.4 , and -115.7 km s^{-1} . We see CH^+ absorption from the -64.5 and -77.6 km s^{-1} components, considering the precision of our velocity scale, but not at the more extreme velocities. In their Fig. 8, Braun & Strom show velocities from -97 to -105 km s^{-1} over an arch-like structure in their field centered on $\alpha = 6^h 14^m 15^s$, $\delta(1950) = 22^\circ 27'$ that is comparable to our high velocity Ca II absorption. The range in Ca II velocities seen toward HD 254477, HD 254577, and HD 43582 suggests a shock velocity of about 100 km s^{-1} for the expanding SNR. This would correspond to the fast J-type shock in the analysis of Snell et al. (2005).

The only really high velocity CH^+ absorption was seen toward HD 254477, where high velocity Ca I and K I features also appeared at comparable velocities. High velocity Ca I was seen toward two other stars (HD 254577 and HD 43582), and K I toward only one other object (HD 254577). These three directions are most closely associated with the clumps seen in molecular gas, but with the absorption probing much lower densities. The next

highest velocity cloud with CH^+ was seen in the direction of HD 43703 at -30 km s^{-1} . We found no detectable CH at high velocities. The presence of high velocity CH^+ without corresponding CH at the same velocity might provide a clue to the origin of interstellar CH^+ , which remains mysterious despite its known presence for decades. In the Vela Remnant, high velocity CH^+ was seen in the background star HD 72088 without a corresponding component in CH (Wallerstein & Gilroy 1992).

4. Conclusions

Our measurements of atomic and molecular absorption toward stars lying behind IC 443 reveal connections to the gas studied via H I and CO emission. The molecular rich diffuse gas has a velocity that associates it with the ambient molecular cloud. Its density is considerably lower than that inferred for the molecular cloud, but this is not unexpected because absorption probes the diffuse envelope of the cloud. High-velocity gas is revealed by Ca II absorption, which along the eastern edge of the nebula spans a range from -120 to $+80 \text{ km s}^{-1}$. This range is similar to that seen in the shocked molecular gas and its associated 21 cm emission. One difference is that individual velocity components in the Ca II spectra are discerned, suggesting that the expanding SNR created a 100 km s^{-1} shock. The densities derived in the analysis of 21 cm emission, $\sim 10 \text{ cm}^{-3}$, probably pertain to the high-velocity gas that we observe. The optical results presented here provide another facet of the interaction between a SNR remnant and a molecular cloud surrounding it and will aid future modeling efforts.

We thank Ron Snell for permission to use a digitized version of the figure in Huang et al. (1986). G.W. acknowledges an enlightening conversation with Bruce Draine regarding the origin of CH^+ . The research by Alec Hirschauer and Tim Means was supported by the Kenilworth Fund of the New York Community Trust. We made use of the SIMBAD database, operated at Centre de Données Astronomiques de Strasbourg, Strasbourg, France.

REFERENCES

- Böhm-Vitense, E. 1981, *ARA&A*, 19, 295
- Braun, R., & Strom, R. G. 1986, *A&A*, 164, 193
- Chevalier, R. A. 1977, *ARA&A*, 15, 175

- Cornett, R. H., Chin, G., & Knapp, G. R. 1977, *A&A*, 54, 889
- Danks, A. C., Federman, S. R., & Lambert, D. L. 1984, *A&A*, 130, 62
- Dickman, R. L., Snell, R. L., Ziurys, L. M., & Huang, Y.-L. 1992, *ApJ*, 400, 203
- Federman, S. R., Strom, C. J., Lambert, D. L., Cardelli, J. A., Smith, V. V., & Joseph, C. L. 1994, *ApJ*, 424, 772
- Huang, Y.-L., Dickman, R. L., & Snell, R. L. 1986, *ApJ*, 302, L63
- Jenkins, E. B., Silk, J., & Wallerstein, G. 1976, *ApJ*, 209, L87
- Jura, M., & Meyer, D. M. 1985, *ApJ*, 294, 238
- Lambert, D. L., Sheffer, Y., & Crane, P. 1990, *ApJ*, 359, L19
- Lambert, D. L., Sheffer, Y., & Federman, S. R. 1995, *ApJ*, 438, 740
- Lavendy, H., Robbe, J. M., Chambaud, G., Levy, R., & Roueff, E. 1991, *A&A*, 251, 365
- Lee, J.-J., Koo, B.-C., Yun, M. S., Stanimirović, S., Heiles, C., & Meyer, M. 2008, *AJ*, 135, 796
- Lien, D. J. 1984, *ApJ*, 284, 578
- McKee, C. F., & Cowie, L. L. 1975, *ApJ*, 195, 715
- Morton, D. C. 1991, *ApJS*, 77, 119
- . 2003, *ApJS*, 149, 205
- Münch, G. 1968, in *Nebulae & Interstellar Matter*, ed. B. M. Middlehurst & L. H. Aller (Univ. Chicago Press), 365
- Najar, F., Ben Abdallah, D., Jaidane, N., & Ben Lakhdar, Z. 2008, *Chem. Phys. Lett.*, 460, 31
- Pan, K., Federman, S. R., Cunha, K., Smith, V. V., & Welty, D. E. 2004, *ApJS*, 151, 313
- Pan, K., Federman, S. R., Sheffer, Y., & Andersson, B.-G. 2005, *ApJ*, 633, 986
- Robbe, J. M., Lavendy, H., Lemoine, D., & Pouilly, B. 1992, *A&A*, 256, 679
- Savage, B. D., Massa, D., Meade, M., & Wesselius, P. R. 1985, *ApJS*, 59, 397

- Scoville, N. Z., Irvine, W. M., Wannier, P. G., & Predmore, C. R. 1977, *ApJ*, 216, 320
- Sheffer, Y., Rogers, M., Federman, S. R., Abel, N. P., Gredel, R., Lambert, D. L., & Shaw, G. 2008, *ApJ*, 687, 1075
- Snell, R. L., Hollenbach, D., Howe, J. E., Neufeld, D. A., Kaufman, M. J., Melnick, G. J., Bergin, E. A., & Wang, Z. 2005, *ApJ*, 620, 758
- Sonnentrucker, P., Welty, D. E., Thorburn, J. A., & York, D. G. 2007, *ApJS*, 168, 58
- Strömgren, B. 1948, 108, 242
- Valencic, L. A., Clayton, G. C., & Gordon K. D. 2004 *ApJ*, 616, 912
- van Dishoeck, E. F. 1984, Ph. D. Thesis, Leiden University
- van Dishoeck, E. F., & Black, J. H. 1982, *ApJ*, 258, 533
- van Dishoeck, E. F., Jansen, D. J., & Phillips, T. G. 1993, *A&A*, 279, 541
- Wallerstein, G., & Gilroy, K. K. 1992, *AJ*, 103, 1346
- Welsh, B. Y., & Sallmen, S. 2003, *A&A*, 408, 545
- Welty, D. E., Hobbs, L. M., & Morton, D. C. 2003, *ApJS*, 147, 61
- Ziurys, L. M., Snell, R. L., & Dickman, R. L. 1989, *ApJ*, 341, 857

Table 1. IC 443 objects

Name	R.A. (2000)	Dec. (2000)	V	$B - V$	Spectral Type	$E(B - V)$	M_V
ALS 8828	06 ^h 16 ^m 13.3 ^s	+22° 45' 48''	10.90	0.60	B2V	0.82	−2.50
HD 254346	06 16 57.3	+22 11 42	9.74	0.39	B2:III:	0.63	−3.60
HD 254477	06 17 26.4	+22 25 38	9.77	0.59	B8V	0.68	0.10
HD 254577	06 17 54.3	+22 24 32	9.19	0.64	B0.5II-III	0.92	−4.95
HD 43582	06 18 00.3	+22 39 29	8.79	0.32	B0IIIn	0.62	−5.00
HD 254700	06 18 25.3	+22 57 34	9.83	0.33	B5V	0.49	−1.00
HD 254755	06 18 31.7	+22 40 45	8.91	0.42	O9Vp	0.73	−4.80
HD 43703	06 18 39.4	+23 00 28	8.65	0.33	B1IV:p	0.59	−4.10
HD 43753	06 18 59.7	+23 00 04	7.89	0.25	B0.5III	0.53	−4.70
HD 43871	06 19 34.5	+22 49 47	8.38	0.05	A0V	0.05	1.00
HD 43907	06 19 45.2	+22 06 38	8.70	0.30	B1V:p	0.56	−3.60

Table 2. Equivalent Widths toward ALS 8828, HD 254346, HD 254477, HD 254577, HD 43582, and HD254700

Line	λ (Å)	ALS 8828		HD 254346		HD 254477		HD 254577		HD 43582		HD 254700	
		W_λ (mÅ)	v_{LSR} (km s ⁻¹)	W_λ (mÅ)	v_{LSR} (km s ⁻¹)	W_λ (mÅ)	v_{LSR} (km s ⁻¹)	W_λ (mÅ)	v_{LSR} (km s ⁻¹)	W_λ (mÅ)	v_{LSR} (km s ⁻¹)	W_λ (mÅ)	v_{LSR} (km s ⁻¹)
C ₂ R(0)	8757.686	5.9(1.3)	-5.4	3.7(2.1)	-2.3	6.3(0.8)	-9.0
C ₂ R(2)	8753.949	2.7	...	5.8(1.7)	-2.7	11.6(1.2)	-8.1
C ₂ Q(2)	8761.194	5.3(1.4)	-5.1	15.1(1.4)	-8.3
C ₂ P(2)	8766.031	5.0(1.9)	-4.2
C ₂ R(4)	8751.686	4.8(1.9)	-12.2	10.7(2.1)	-1.9	7.8(1.3) ^a	-7.5
C ₂ Q(4)	8763.751	7.1(1.0)	-6.8	7.4(2.2)	-2.9	6.3(2.8)	+0.1	16.7(1.1)	-8.1
C ₂ P(4)	8773.430	4.0(1.2)	-6.7
C ₂ R(6)	8750.848	4.9(1.0)	-6.1
C ₂ Q(6)	8767.759	4.8(1.9)	-3.8	8.2(1.0)	-6.5
C ₂ P(6)	8782.308	3.4(0.8)	-6.8
C ₂ Q(8)	8773.221	3.4(1.4) ^b	6.1(1.2)	-6.7
C ₂ P(8)	8792.648	2.5(1.0)	-6.4
C ₂ Q(10)	8780.141	3.4(0.9)	-7.2
CN R(0)	3874.610	12.7(1.8)	-9.2	10.7(1.0)	-5.7	13.6(1.7)	-1.5	24.4(1.2)	-9.4
CN R(1)	3874.000	2.9(0.8)	-6.2	8.4(1.8)	-2.2	13.4(1.2)	-7.9
CN P(1)	3875.760	6.5(1.5)	-1.1	7.1(1.1)	-9.2
CH A - X	4300.313	42.3(1.3)	-8.5	21.7(0.8)	-3.8	28.0(1.7)	-2.0	23.4(0.6)	-7.0	12.1(0.4)	-8.9	10.6(0.9)	-4.6
...	4.2(0.6)	+8.6	3.6(1.7)	+12.8	2.2(0.6)	+9.7	3.3(0.4)	+5.9
CH B - X	3890.217	11.6(2.1)	-9.1	3.0(0.7)	-7.2	3.2(0.5)	-9.5
CH B - X	3886.409	14.3(3.1)	-8.5	9.8(2.1)	-0.7	5.6(2.2)	-1.1	4.4(0.8)	-7.3	2.8(0.4)	-9.5	4.3(1.6)	-2.1
CH B - X	3878.774	2.2(0.7)	-4.4
CH ⁺ (0-0)	4232.548	22.5(1.6)	-7.9	11.4(0.7)	-4.9	4.2(1.8)	-74.5	2.1(0.5)	-19.4	19.9(0.4)	-8.8	15.4(0.8)	-4.3
...	...	11.0(1.6)	+5.9	15.8(0.8)	+9.2	4.3(1.8)	-61.1	19.0(0.5)	-5.4	4.4(0.4)	+3.1	4.7(0.9)	+8.4
...	13.8(2.2)	+1.2	6.8(0.5)	+9.2
CH ⁺ (1-0)	3957.692	12.9(2.5)	-8.6	6.4(1.2)	-3.8	5.7(2.6)	-1.6	10.4(0.9)	-6.8	8.9(0.6)	-8.2	6.9(1.2)	-4.3
...	6.6(1.1)	+9.0	3.7(0.9)	+14.2	2.2(0.6)	+3.1	2.2(1.2)	+8.4
Ca II K	3933.663	138(3)	-7.9	12.8(1.6)	-75.0	39.9(2.3)	-118.1	78.4(1.0)	-110.8	16.6(0.8)	-107.8	14.3(1.6)	-24.9
...	...	131(3)	+5.6	236(2)	-2.2	154(2)	-91.4	184(1)	-58.7	45.8(0.8)	-91.5	115(1)	-5.0
...	87.2(1.8)	+12.3	133(2)	-77.6	183(1)	-41.9	106(1)	-71.8	104(1)	+7.1
...	144(2)	-64.5	179(1)	-23.7	164(1)	-59.7	36.7(1.3)	+15.3
...	142(2)	-50.6	184(1)	-7.1	176(1)	-42.9
...	97.4(2.3)	-38.4	189(1)	+10.3	156(1)	-26.8
...	161(2)	-20.3	157(1)	-8.9
...	153(2)	-3.4	152(1)	+6.2

Table 2—Continued

...	151(2)	+11.4	62.6(0.5)	+36.4
...	8.0(0.5)	+79.5
Line	λ (Å)	ALS 8828		HD 254346		HD 254477		HD 254577		HD 43582		HD 254700	
		W_λ (mÅ)	v_{LSR} (km s ⁻¹)										
Ca II H	3968.468	116(3)	-7.9	4.7(1.3)	-74.0	8.6(2.4)	-115.7	43.3(0.7)	-110.9	5.7(0.6)	-107.2	4.5(2.1)	-29.5
	...	109(3)	+4.8	171(2)	-2.5	120(3)	-90.4	164(1)	-57.3	23.0(0.6)	-90.9	82.2(1.4)	-4.3
	65.6(1.5)	+9.8	130(3)	-77.7	164(1)	-41.8	81.5(0.6)	-70.2	72.5(1.4)	+7.8
	130(3)	-64.8	160(1)	-21.7	129(1)	-58.4	14.5(1.4)	+16.4
	117(3)	-50.7	159(1)	-6.4	150(1)	-41.5
	59.3(3.4)	-38.1	154(1)	+9.8	108(1)	-25.6
	108(3)	-20.1	125(1)	-7.7
	121(3)	-3.0	91.3(0.6)	+7.1
	105(3)	+10.4	37.9(0.4)	+36.4
	5.5(0.5)	+79.8
Ca I	4226.728	4.9(1.6)	-14.1	8.8(0.7)	-1.2	51.4(3.1)	-72.6	13.3(0.8)	-55.8	6.2(0.7)	-63.6	8.7(1.2)	-4.7
	...	11.0(1.7)	-1.3	2.5(0.7)	+11.3	8.0(3.1)	-59.2	18.1(0.8)	-46.7	12.8(0.7)	-40.8	9.2(1.2)	+7.6
	11.9(2.3)	-1.1	8.7(0.6)	-21.8	8.0(0.7)	-10.2
	19.9(0.6)	-7.5	2.2(0.7)	+3.6
	6.9(0.6)	+10.3
K I	7698.974	216(2)	-8.1	176(1)	-1.4	9.5(2.3)	-82.7	7.9(1.1)	-55.4	127(2)	-9.1	134(2)	-5.2
	...	51.8(1.9)	+5.7	51.1(1.2)	+9.9	45.4(2.3)	-65.0	14.4(1.1)	-46.9	25.0(1.6)	+5.5	30.3(1.5)	+6.9
	12.0(2.3)	-52.6	7.0(1.2)	-20.1	9.3(1.5)	+15.7
	170(2)	-1.5	221(1)	-5.9
	23.9(2.2)	+10.0	33.3(1.2)	+8.6

^aMay include absorption from R(8).^bMay include absorption from P(4).

Table 3. Equivalent Widths toward HD 254755, HD 43703, HD 43753, HD 43871, and HD 43907

Line	λ (Å)	HD 254755		HD 43703		HD 43753		HD 43871		HD 43907	
		W_λ (mÅ)	v_{LSR} (km s ⁻¹)								
C ₂ R(0)	8757.686	2.5(0.7)	-6.7
C ₂ R(2)	8753.949	5.6(0.9)	-3.8
C ₂ Q(2)	8761.194	5.3(0.9)	-4.7
C ₂ P(2)	8766.031	1.9(0.8)	-2.7
C ₂ R(4)	8751.686	3.5(0.9)	-6.8
C ₂ Q(4)	8763.751	10.2(1.2)	-5.7	7.5(1.3)	-3.3	5.4(1.3)	-5.4
C ₂ P(4)	8773.430	2.6(0.9)	-5.6
C ₂ Q(6)	8767.759	2.8(0.8)	-5.3
C ₂ Q(8)	8773.221	3.1(0.9)	-4.8
C ₂ Q(10)	8780.141	3.2(1.0)	-8.1
CN R(0)	3874.610	7.8(0.6)	-6.3	2.2(0.4)	-5.7	2.0(0.6)	-12.2
CN R(1)	3874.000	4.2(0.7)	-7.0	1.6(0.5)	-10.1
CH A - X	4300.313	25.6(0.5)	-6.0	20.0(0.6)	-5.8	10.4(0.7)	-5.4	10.9(1.1)	-10.0
...	...	2.7(0.5)	+5.0	5.1(1.1)	+2.4
CH B - X	3890.217	5.1(0.6)	-6.7	2.8(0.6)	-5.1
CH B - X	3886.409	7.2(0.6)	-3.9	4.0(0.6)	-6.3	3.2(0.8)	-11.6
...	...	1.1(0.6)	+8.9	1.5(0.8)	-1.8
CH ⁺ (0-0)	4232.548	25.1(0.5)	-6.5	2.4(0.5)	-30.8	3.4(1.8)	-20.4	11.4(0.8)	-7.8
...	...	3.8(0.5)	+8.7	27.2(0.6)	-6.3	16.1(1.4)	-5.6	8.0(0.8)	+0.4
...	4.3(0.7)	+6.9
CH ⁺ (1-0)	3957.692	15.2(0.5)	-6.4	12.3(0.7)	-6.5	9.4(1.5)	-7.0	10.2(1.3)	-4.7
...	...	2.7(0.5)	+7.2	2.2(0.6)	+3.1	4.3(1.3)	+0.2
Ca II K	3933.663	15.2(1.0)	-74.7	4.1(1.0)	-36.2	122(2)	-15.1	92.3(0.8)	-4.2	20.0(1.0)	-78.8
...	...	47.6(1.3)	-24.9	152(1)	-6.0	114(2)	-1.6	8.2(0.5)	+5.8	5.2(0.9)	-64.3
...	...	152(1)	-7.3	134(1)	+8.1	108(2)	+8.7	131(1)	-10.2
...	...	151(1)	+7.3	140(1)	+2.6
Ca II H	3968.468	7.8(0.9)	-77.2	6.4(1.0)	-31.9	68.0(1.5)	-15.6	41.9(0.9)	-4.3	10.3(1.1)	-78.9
...	...	25.4(1.1)	-24.6	120(1)	-5.6	105(2)	-2.3	4.6(0.8)	+6.9	3.0(0.7)	-63.3
...	...	124(1)	-5.5	95.8(1.0)	+7.9	63.6(1.5)	+8.6	91.5(1.3)	-10.0
...	...	90.0(1.1)	+7.4	117(1)	+1.7
Ca I	4226.728	12.4(0.7)	-5.5	10.6(0.6)	-6.3	7.5(1.0)	-19.1	6.0(0.8)	-9.0
...	5.4(0.6)	+6.9	6.6(1.0)	-1.2	9.2(0.8)	+2.9
K I	7698.974	158(1)	-5.0	194(1)	-5.5	14.3(1.3)	-18.1	2.7(0.8)	+5.9	107(1)	-10.7
...	...	42.9(0.8)	+9.3	25.2(1.0)	+6.8	118(1)	-3.9	68.5(1.0)	-0.2

Table 3—Continued

... .. 27.9(1.3) +5.4

Table 4. C_2 Results

J	$N(J)$ (10^{12} cm $^{-2}$)						
	ALS 8828	HD 254346	HD 254477	HD 254577	HD 254755	HD 43703	HD 43907
0	8.9 ± 2.0	5.5 ± 3.2	...	9.5 ± 1.2	3.7 ± 1.1
2	14 ± 3	25 ± 7	...	46 ± 4	19 ± 2
4	21 ± 4	32 ± 6	19 ± 9	46 ± 3	23 ± 3	23 ± 4	16 ± 4
6	...	14 ± 6	...	25 ± 2	8.3 ± 2.4
8	18 ± 3	9.2 ± 2.7
10	10 ± 3	9.5 ± 3.0

Table 5. Component Structure

v_{LSR} km s ⁻¹	$N(\text{Ca II})$ 10 ¹¹ cm ⁻²	$N(\text{Ca I})$ 10 ⁹ cm ⁻²	$N(\text{K I})$ 10 ¹¹ cm ⁻²	$N(\text{CH}^+)$ 10 ¹² cm ⁻²	$N(\text{CH})$ 10 ¹² cm ⁻²	$N(\text{C}_2)$ 10 ¹² cm ⁻²	$N(\text{CN})$ 10 ¹² cm ⁻²
ALS 8828							
-7.9	52 – 120	18 ± 7	130 ± 10	30 ± 3	72 ± 3	66 ± 14	4.6 ± 0.8
+5.6	45 – 100	43 ± 8	3.6 ± 0.2	13 ± 3
HD 254346							
-75.0	1.4 ± 0.2
-2.2	52 – 59 4.6 ± 0.8	34 ± 3	41 ± 1	14 ± 1	30 ± 2	94 ± 25	3.5 ± 0.5
+12.3	20 – 28	9.2 ± 2.6	3.5 ± 0.1	20 ± 1	5.2 ± 0.8
HD 254477							
-118.1	4.1 ± 0.3
-91.4	42 – 59
-77.6	> 980	290 ± 30	0.55 ± 0.14	4.9 ± 2.2
-64.5	100 – 700	30 ± 13	3.1 ± 0.2	5.0 ± 2.2
-50.6	49 – 83	...	0.70 ± 0.15
-38.4	12 – 17
-20.3	28 – 34
-3.4	44 – 64	47 ± 10	36 ± 2	16 ± 3	40 ± 3	63 ± 30	6.7 ± 1.1
+11.4	29 – 35	...	1.5 ± 0.2	...	4.4 ± 2.2
HD 254577							
-110.8	8.9 – 10.0
-58.7	170 – 230	53 ± 4	0.46 ± 0.07
-41.9	170 – 280	74 ± 4	0.85 ± 0.07
-23.7	160 – 270	33 ± 3	0.40 ± 0.07	2.4 ± 0.6
-7.1	110 – 140	83 ± 3	150 ± 10	24 ± 1	32 ± 1	154 ± 17	11 ± 1
+10.3	73 – 83	26 ± 2	2.1 ± 0.1	8.1 ± 0.6	2.7 ± 0.8
HD 43582							
-107.8	1.6 ± 0.1
-91.5	5.2 ± 0.1
-71.8	29 – 33
-59.7	52 – 88	23 ± 3
-42.9	86 – 110	50 ± 3
-26.8	31 – 33
-8.9	52 – 60	30 ± 3	15 ± 1	26 ± 1	16 ± 1
+6.2	22 – 23	8.1 ± 2.6	1.5 ± 0.1	5.2 ± 0.5	4.0 ± 0.5
+36.4	9.0 – 10.0
+79.5	0.99 ± 0.05
HD 254700							
-24.9	1.5 ± 0.2
-5.0	24 – 28	33 ± 5	17 ± 1	18 ± 2	14 ± 2
+7.1	20 – 23	35 ± 5	1.9 ± 0.1	5.4 ± 1.0
+15.3	4.1 ± 0.1	...	0.54 ± 0.09
HD 254755							
-74.7	1.7 ± 0.1
-24.9	5.6 ± 0.1
-7.3	59 – 67	49 ± 3	27 ± 1	35 ± 1	37 ± 1	73 ± 15	3.2 ± 0.5
+7.3	21 – 22	...	2.9 ± 0.1	4.8 ± 0.5	3.4 ± 0.6

Table 5—Continued

v_{LSR} km s ⁻¹	$N(\text{Ca II})$ 10 ¹¹ cm ⁻²	$N(\text{Ca I})$ 10 ⁹ cm ⁻²	$N(\text{K I})$ 10 ¹¹ cm ⁻²	$N(\text{CH}^+)$ 10 ¹² cm ⁻²	$N(\text{CH})$ 10 ¹² cm ⁻²	$N(\text{C}_2)$ 10 ¹² cm ⁻²	$N(\text{CN})$ 10 ¹² cm ⁻²
HD 43703							
-36.2	0.68 ± 0.10	2.8 ± 0.6
-6.0	48 – 55	41 ± 3	67 ± 2	35 ± 1	27 ± 1	77 ± 13	1.0 ± 0.3
+8.1	29 – 32	20 ± 3	1.6 ± 0.1	5.0 ± 0.8
HD 43753							
-15.1	14 – 16	28 ± 4	0.85 ± 0.05	4.0 ± 2.1
-1.6	>100	25 ± 4	13 ± 1	20 ± 2	13 ± 1
+8.7	14 – 16	...	1.7 ± 0.1
HD 43871							
-4.2	9.6 ± 0.2	...	0.15 ± 0.05
+5.8	0.94 ± 0.06
HD 43907							
-78.8	2.3 ± 0.1
-64.3	0.62 ± 0.08
-10.2	26 – 29	23 ± 4	10 ± 1	15 ± 1	14 ± 2	53 ± 13	0.68 ± 0.21
+2.6	59 – 74	35 ± 4	5.2 ± 0.1	9.6 ± 0.9	6.4 ± 1.3

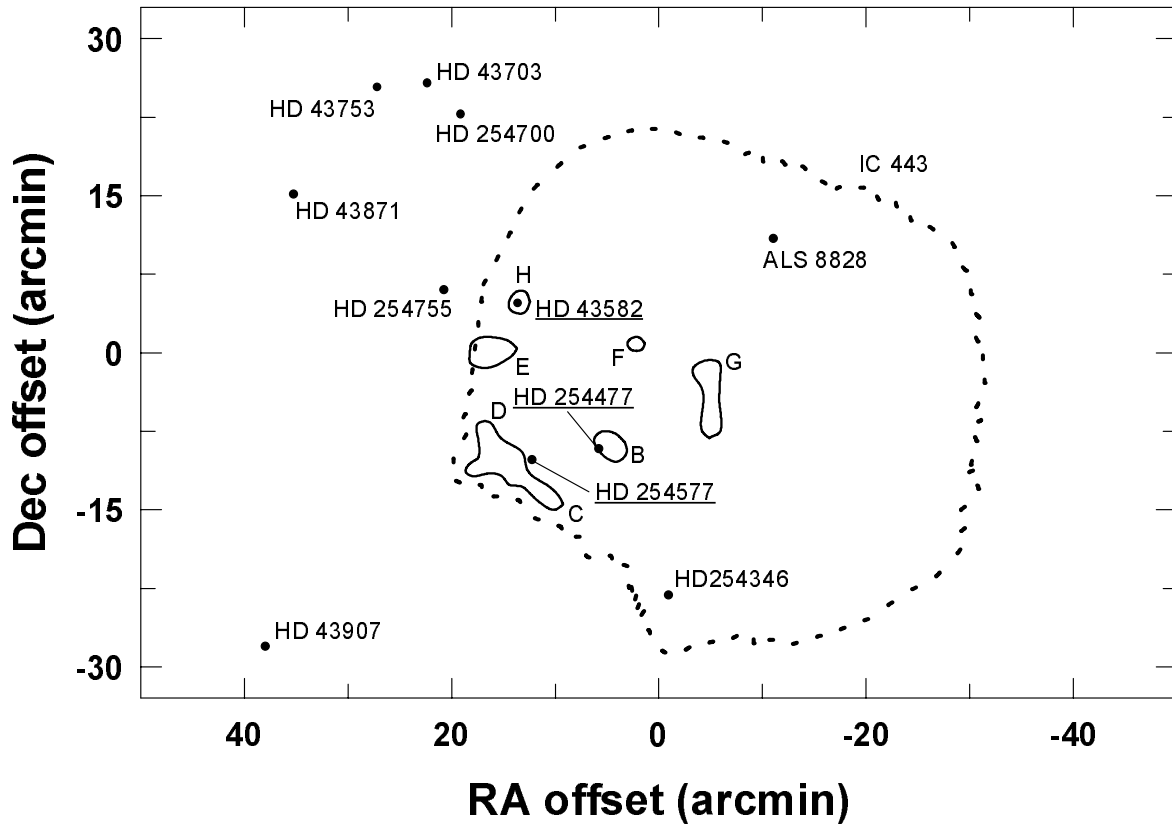


Fig. 1.— Map showing the relationship between IC 443, the molecular clumps noted by Huang et al. (1986) and shown by solid contours, and the directions analyzed here labeled by HD numbers. The dashed line indicates the extent of the radio continuum emission. Underlined HD numbers are sight lines with Ca II absorption spread over 100 km s^{-1} (§3.3). The offsets are relative to RA(1950) = $6^h 14^m$ and DEC(1950) = $22^\circ 36'$.

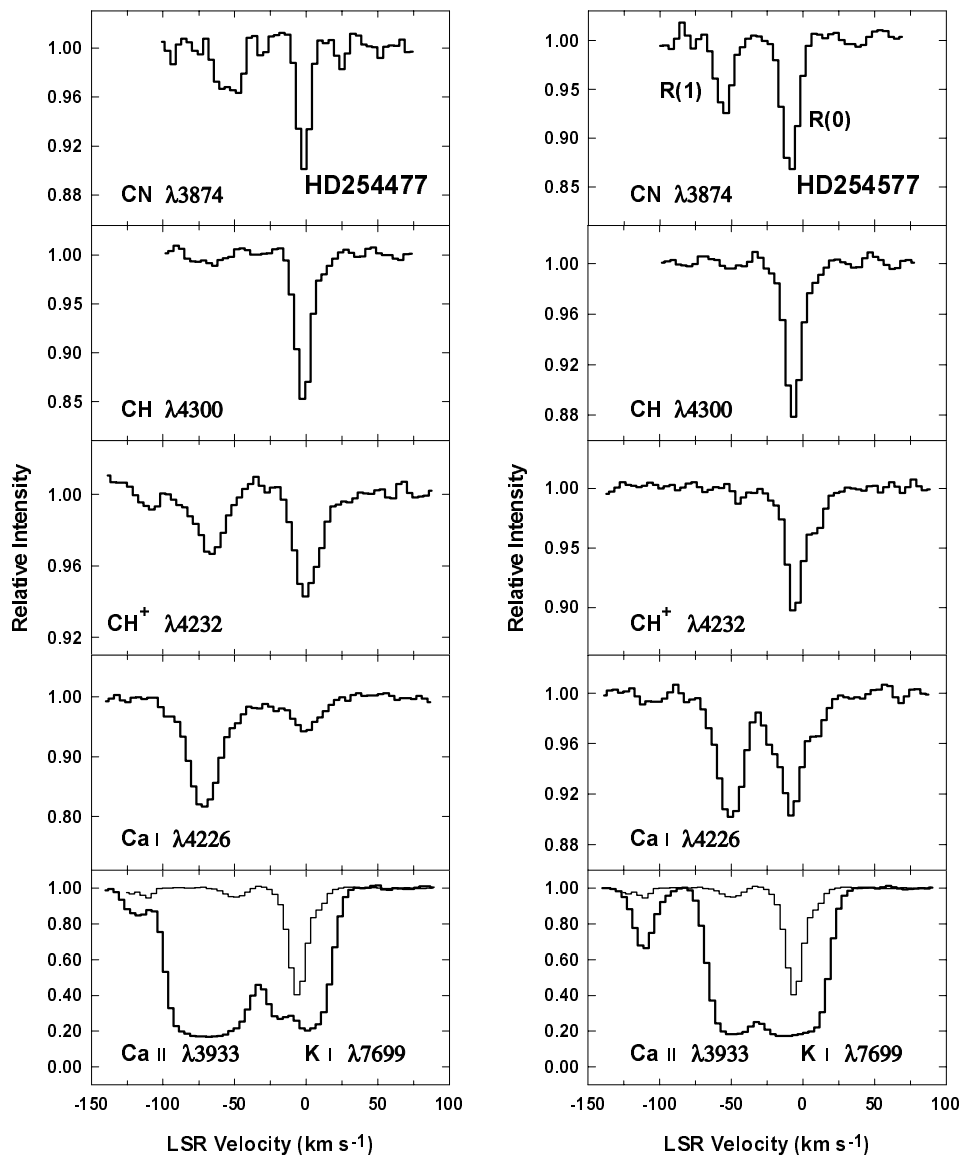


Fig. 2.— Spectra showing CN, CH, CH⁺, Ca I, Ca II, and K I absorption toward HD 254477 and HD 254577. K I $\lambda 7699$ is indicated by the thin line in the bottom panel, showing the different velocity ranges probed by neutral and ionized gas. The K I features near -125 km s^{-1} are telluric. The individual panels have different vertical scales.

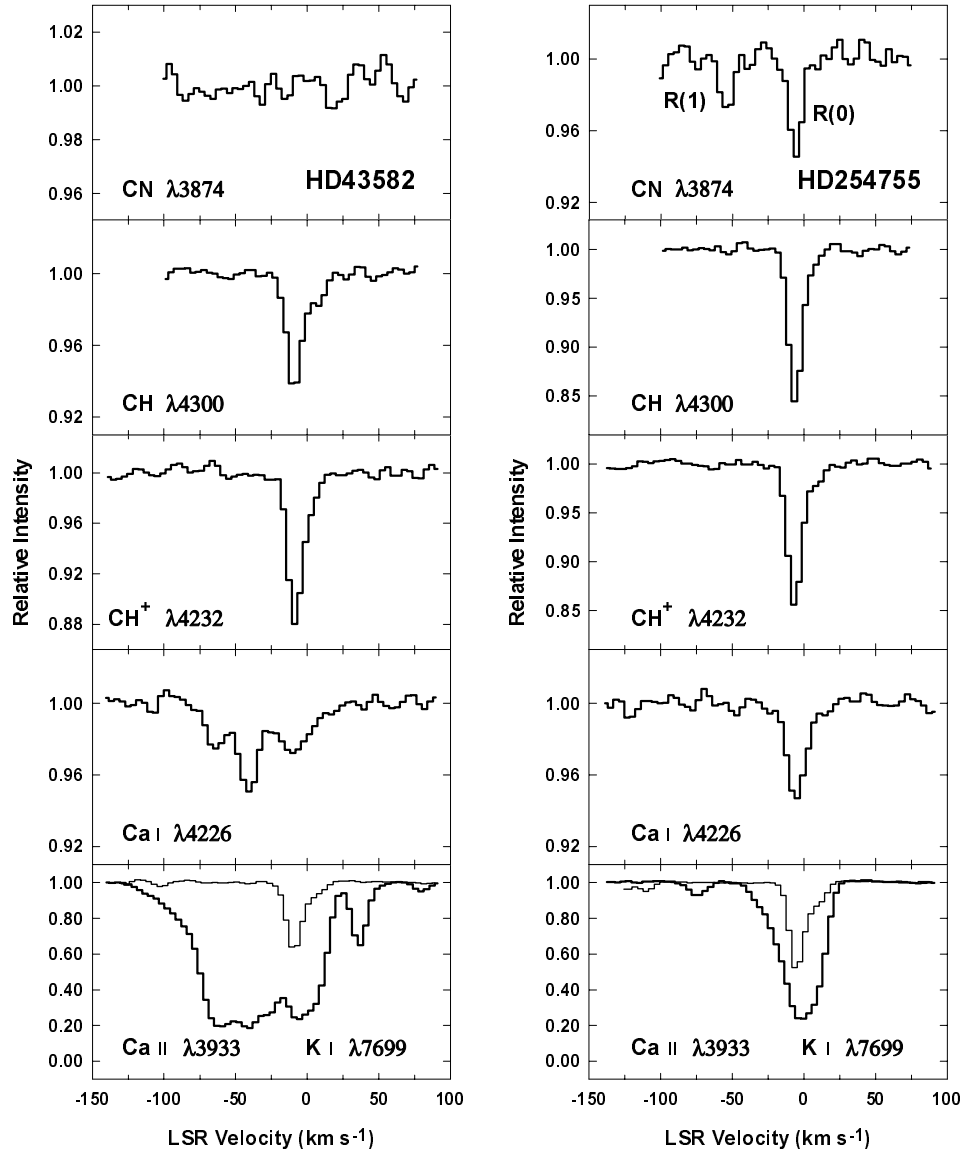


Fig. 3.— Same as Fig. 2 for HD 43582 and HD 254755.

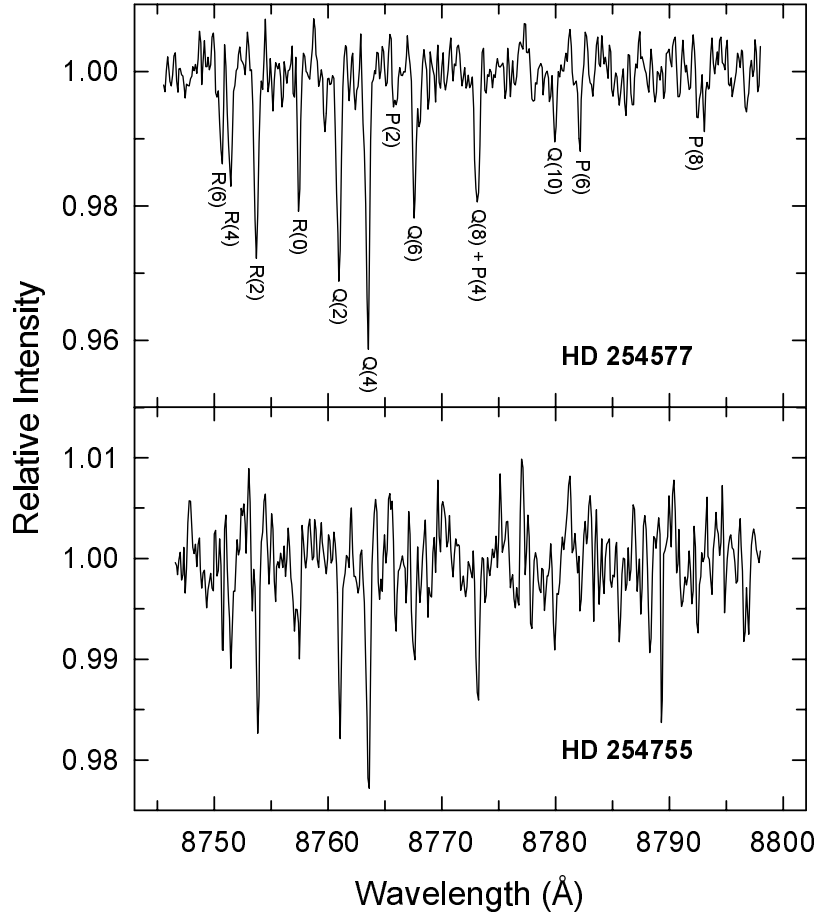


Fig. 4.— C₂ spectra toward HD 254577 and HD 254755. The features to the right of the P(8) line in the top panel and near 8790 Å in the bottom are instrumental artefacts.